Progress In Electromagnetics Research C, Vol. 130, 241–254, 2023

Angle Independent Metamaterial Absorber for S and C Band Application

Goriparthi Rajyalakshmi[1, *], Yada Ravikumar[2], Dasari R. Krishna[1], and Kumbha S. Rao[2]

Abstract—In this paper, the development and design of angle independent Metamaterial Microwave Absorbers (MMAs) are presented. The unit cell consists of four trapezoids that are linked by consolidated resistors with coextensive squares. The absorber is built on a dielectric substrate (FR4) with a thickness of 0.256 mm ($\lambda/144$) and a dielectric constant of 4.3. The wideband absorption is acquired in the range of 2.21 to 6.61 GHz with a wide band of 4.40 GHz with absorptivity above 90%. In the area of interest, a flat band is obtained, and to examine the current distribution and electric field in the respective region two peaks are considered at a frequency of 2.49 and 5.68 GHz, with maximum absorptivity of 92.50% and 92.14%, respectively. The presented absorber is examined under different angles for phi and theta variation. From the phi variation, it is observed that for all the angles absorptivity does not vary which confirms that the absorber acts as an angle independent. The fabricated sheet consists of an array of a unit cell, which is examined inside an anechoic chamber with the help of two horn antennas and Vector VNA. The tested and simulated results are compared, and it was observed that they are in close agreement. At last, the presented and already reported MMAs are compared, and it is observed that the presented one operates for the low frequency with higher bandwidth. The presented absorber can be practically used for defense applications for Radar Cross Sections (RCS) reduction.

1. INTRODUCTION

For decennary, structures grounded on metamaterials have attracted the attention of analysts in several scientific fields, such as electronics, physics, microwaves, and more. This topic has originated utilization worldwide in absorbers, filters, medical devices, communication systems, resonators, antennas, polarization conversion, couplers, sensor, smart solar control, etc. The electromagnetic (EM) wave response in some of these applications can be manually tuned by modifying the EM parameters and by delineating the unit cell structure using sub-wavelength values, i.e., values of effective permittivity (ε_{eff}) and permittivity (μ_{eff}) [1]. The research on planar structures based on metamaterials has been focused on absorbers, i.e., absorbers whose surface can administer and modify EM waves.

Previously, the absorption of EM waves was performed by the traditional method, which was massive and operated in a narrow frequency band with respect to volume [2]. To conquer bandwidth limitations, metamaterial structures have been proposed and considered in the literature. By changing the incident wave via reflection or via transmission from the metamaterial, absorption could be attained [3]. Absorption can be achieved by creating a two-dimensional periodic arrangement of bi-anisotropic metallic elements laid over some dielectric [4]. Various systems are used to operate in the distinct frequency domain. For example, Circular Split Ring Resonators (CSRRs) have been used for the infrared emission [5]. The nanotubes are used for the visible range [6], Self-Complementary Rings

Received 5 December 2022, Accepted 14 February 2023, Scheduled 2 March 2023
* Corresponding author: Goriparthi Rajyalakshmi (rajyalakshmi.gori@gmail.com).
[1] Department of ECE, Osmania University, Hyderbad, Telangana, India. [2] DLRL DRDO, Hyderbad, Telangana, India.

(SCRs) [7], and the double tip is designed for the microwave range [8]. Metal grating is used for the Terahertz (THz) range [9]. An innovative Electromagnetic Band Gap (EBG) metamaterial structure is introduced with low-complexity unit-cell fabrication using an easy concept of inductive serpentine lines and interdigital capacitors [10]. A dense ternary band ($\lambda/135.66$) allows ultra-thin absorbers to be used for S-, C-, and X-band applications [11].

Through various design methods, the absorption band for metamaterials can be increased, such as multi-layer structures composed of metal-dielectric structures in order to produce multiple plasmonic resonances [12], wrapped CSRR (normal incidence only) [13], and single-layer structure designs to induce multi-plasmon resonance. Single layer structure is designed to achieve broader bandwidth with the help of neighbouring plasmonic resonances, but it does not operate for oblique incidence [14].

The presented absorber focused on angle independent MMA. It is composed of four trapezoids linked by consolidated resistors into coextensive and diagonal squares. The absorption efficiency reached greater than 90% between 2.21 and 6.61 GHz. The flat response is obtained in the mentioned frequency range. For analysis purpose, two different frequency peaks are considered at 2.49 and 5.68 GHz with absorptivity of 92.50% and 92.14%, respectively. The structure is optimizes w.r.t substrate height, spacer height, and resistance. The combination of best optimized results is obtained and plotted in the respective figure. To satisfy the metamaterial properties, the effective parameters are used and plotted for real and imaginary parts of ε and μ versus frequency in Figures 9 and 10, respectively. It is observed from the plots that ε and μ vary in the range of interest which satisfies the properties of metamaterials. The structure is further examined at different angles for phi and theta variation. For phi absorptivity plot remains constant for all the angle variation; therefore, the presented absorber is angle independent. The fabricated sheet which consists of array of unit cell is examined inside an anechoic chamber with the help of two horn antennas and VNA. The result obtained from the chamber is compared with the simulated one, and it is observed that they are in close agreements. At last, the presented and already reported state of arts are compared, and it is found that the presented one is used for low frequency with wide bandwidth. The presented MMA finds practical applications in the field of defence for Radar Cross Sections (RCS) reduction.

2. DESIGN OF THE STRUCTURE

The presented MMA unit cell contains 4 trapezoids connected via consolidated resistors to coextensive square. The overall measurement of 12 mm × 12 mm is depicted in Fig. 1. The system consists of four

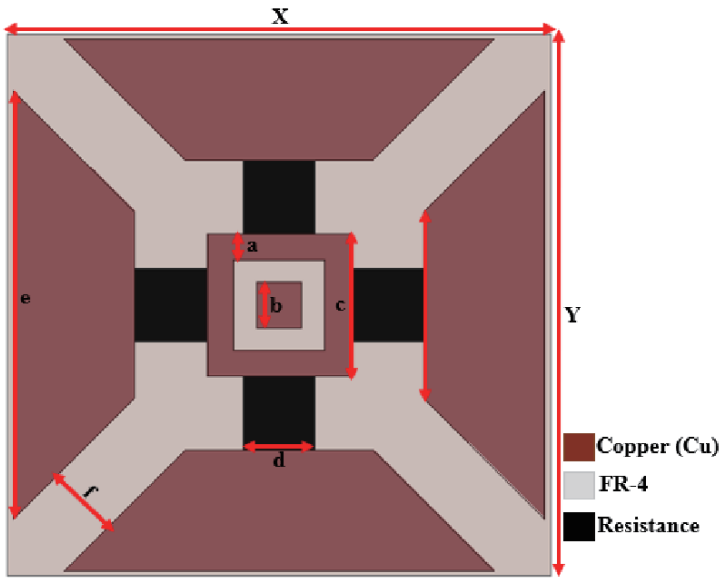

Figure 1. Frontage of suggested MMA unit cell.

surfaces. The uppermost (resonating) and lowermost surfaces are composed of conducting material (Cu, conductivity $\sigma = 5 \times 10^{-7}$ S, thickness = 0.0.5 mm). The second one is a dielectric substrate (FR_4, $\varepsilon_r = 4.4$, $\delta = 0.02$, thickness = 1.6 mm), and the tertiary surface is as air aperture, which is used to obtain flat band in the area of interest with absorptivity greater than 90%. The systematic diagram of different surfaces is shown in Fig. 2.

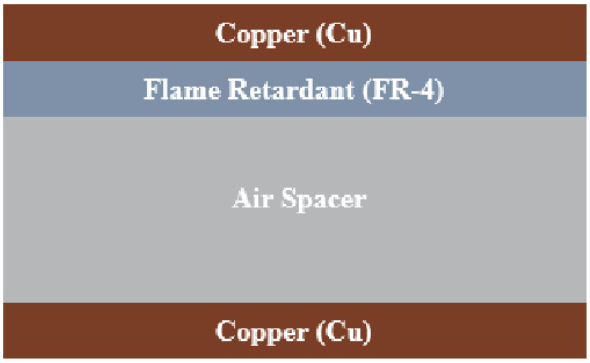

Figure 2. Graphic representation of suggested MMA.

3. SIMULATION AND PARAMETRIC ANALYSIS

The unit cell design has been depicted in Fig. 1. The presented absorber is simulated using ANSYS HFSS 19.1, which is a commercially available software. The best values of variables used in the structure in terms of millimetres are as follows: $X = Y = 12$, $a = 0.58$, $b = 1$, $c = 3.16$, $d = 1.6$, $e = 9.46$, and $f = 1.6$. The MMA is optimized with respect to the height of substrate, height of air aperture,s and resistance, respectively. Firstly, the height of substrate varies from 0.3 to 0.7 mm in the step size of 0.1. For 0.5 mm wider band is achieved which covers the range of interest, i.e., S and C bands as portrayed in Fig. 3. Secondly, the height of air aperture varies from 8 to 12 mm in the step size of 1. For 10 mm best absorptivity result with flat response is obtained compared to other variation as portrayed in Fig. 4. At last, consolidated resistance varies in the range of 40 to 70 Ω in the step size of 10. For the value of 66 Ω wider band is achieved as portrayed in Fig. 5.

The optimized parameter obtained to achieve wider band with flat response is portrayed in Fig. 6, where the height of substrate, height of air aperture, and consolidated resistance values are 0.5 mm, 10 mm, and 66 Ω, respectively.

The presented structure is simulated with and without consolidated resistance and portrayed in Fig. 7. It is observed from the figure that the structure without resistance has wide band, but its absorptivity is below 1%, and it cannot be considered as an absorber. The structure is again simulated with resistance and absorptivity increase above 90% with flat response in the area of interest.

Equation (1) is used to calculate the absorptivity, where S_{11} and S_{21} are the reflection and transmission coefficients. However, the lower surface is fully covered with copper; therefore, the transmitted coefficient S_{21} becomes zero in Equation (1), and absorptivity fully depends upon S_{11}. The lower the value of S_{11} is, the higher the absorptivity will be and vice versa as shown in Equation (2).

$$A(\omega) = 1 - |S_{11}(\omega)|^2 - |S_{21}(\omega)|^2 \quad (1)$$

$$A(\omega) = 1 - |S_{11}(\omega)|^2 \quad (2)$$

The geometry presented has a flat response of 4.4 GHz from 2.21 to 6.61 GHz, with two maximum peaks, i.e., 2.49 and 5.68 GHz are considered for the analysis purpose. The Full Width Half Maxima (FWHM) of 7.43 GHz is obtained from 1.39 to 8.82 GHz and plotted in Fig. 7.

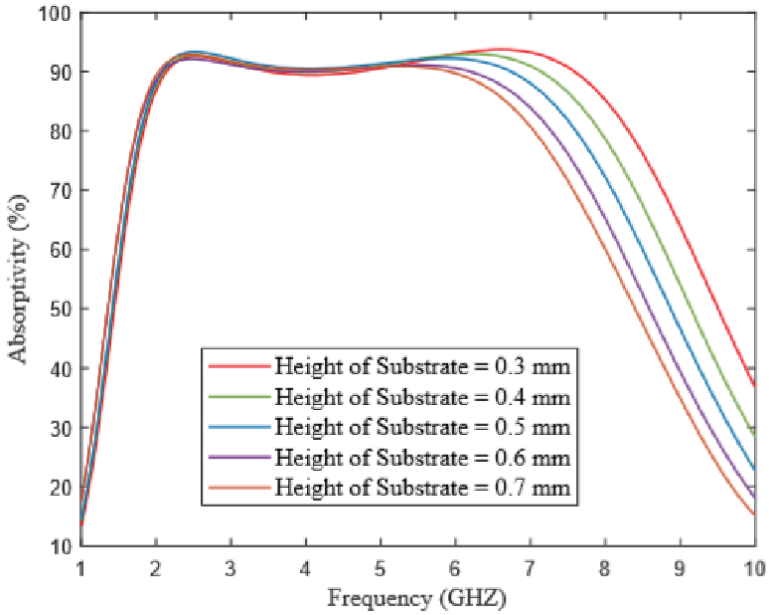

Figure 3. Variation w.r.t height of substrate.

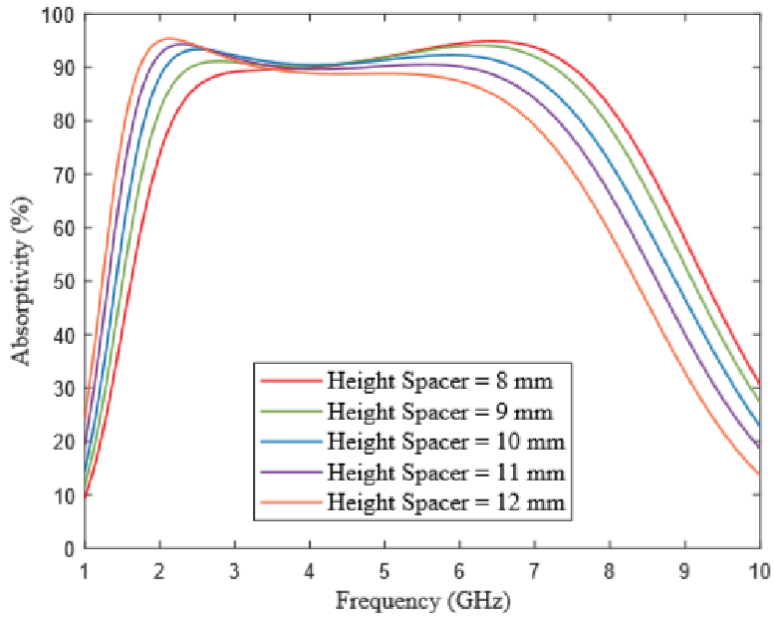

Figure 4. Variation w.r.t height of air apertures.

4. ABSORPTION PHENOMENON

Considering MMA as congruent medium, the phenomenon of absorption can be described. To determine normalized impedance Equation (3) is considered.

$$Z = \sqrt{\frac{(1+S_{11})^2 - S_{21}^2}{(1-S_{11})^2 + S_{21}^2}} \tag{3}$$

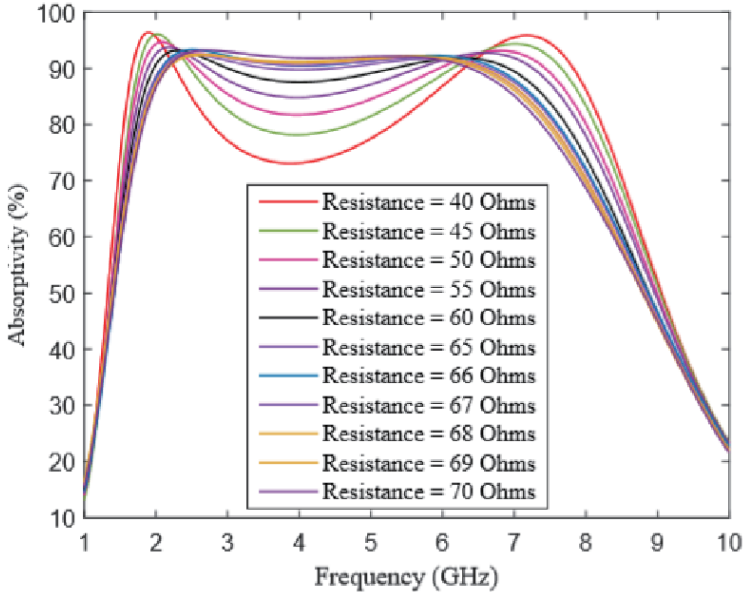

Figure 5. Variation w.r.t consolidated resistance.

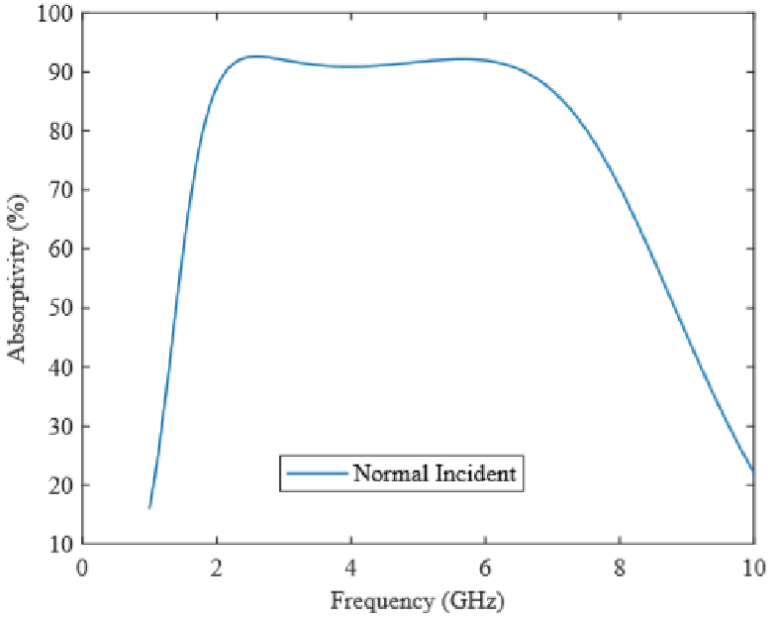

Figure 6. Plot of frequency versus absorptivity.

As bottom surface is completely covered with copper, transmitted power (S_{21}) is 0.

$$Z = \frac{(1 + S_{11})}{(1 - S_{11})} \tag{4}$$

However, to determine Z, S_{21} plays a vital role. Therefore, the small amount of lowermost surface is etched from the all corners in such a way that absorptvity plot remains the same. In Fig. 8, the resulting Z is shown, and at the highest absorption (2.46 and 5.68 GHz) we observe that the imaginary and real parts approach zero and one, respectively. Perfect impedance is achieved, and it has been shown to lead to the highest absorption.

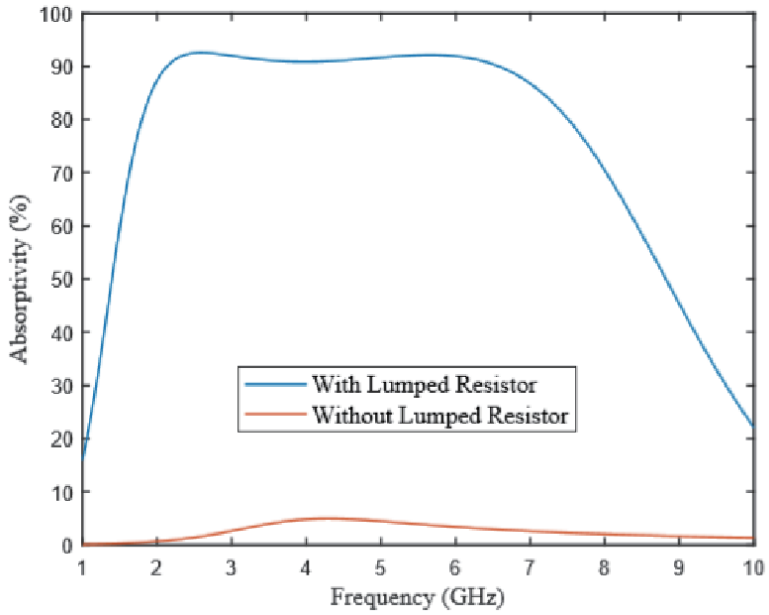

Figure 7. Different cases absorptivity — with and without consolidated resistor.

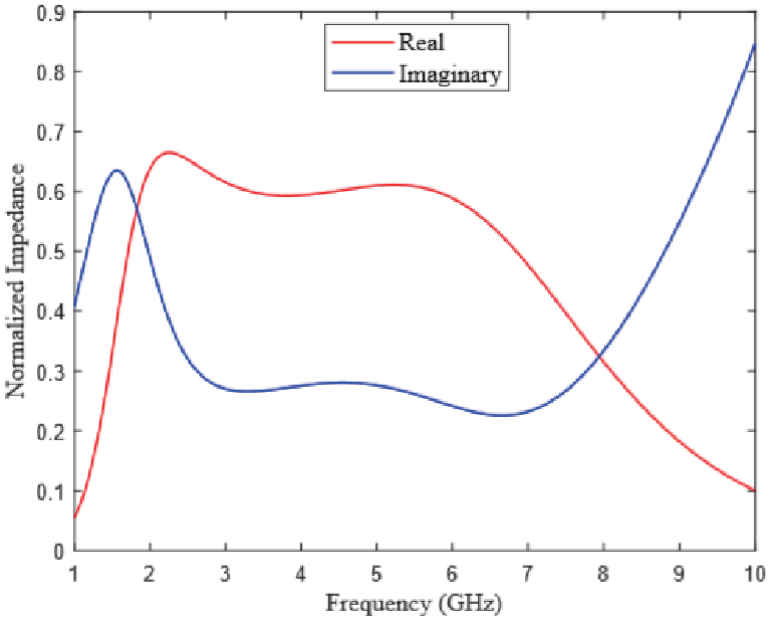

Figure 8. Simulated normal impedance.

In Fig. 8, a rapid change in the values of ε_{eff} and μ_{eff} at the absorption frequency causes the real part to appear and approach unity, satisfying the electrical and magnetic resonance conditions. This can be seen from the ε_{eff} and μ_{eff} plots depicted in Figs. 9 and 10.

As stated in Equations (5)–(8), the effective ε_{eff} and μ_{eff} are determined by using the electrical susceptibility (Es) and magnetic susceptibility (Ms), where d is the distance traveled by the incident EM wave and k is the wave number.

$$E_s = \frac{2jS_{11} - 1}{kS_{11} + 1} \tag{5}$$

$$E_s = \frac{2jS_{11}+1}{kS_{11}-1} \tag{6}$$

$$\varepsilon_{eff} = 1+\frac{E_s}{d} \tag{7}$$

$$\mu_{eff} = 1+\frac{M_s}{d} \tag{8}$$

By using Equation (9), the refractive index (η) is calculated and plotted in Fig. 11. Resonance conditions

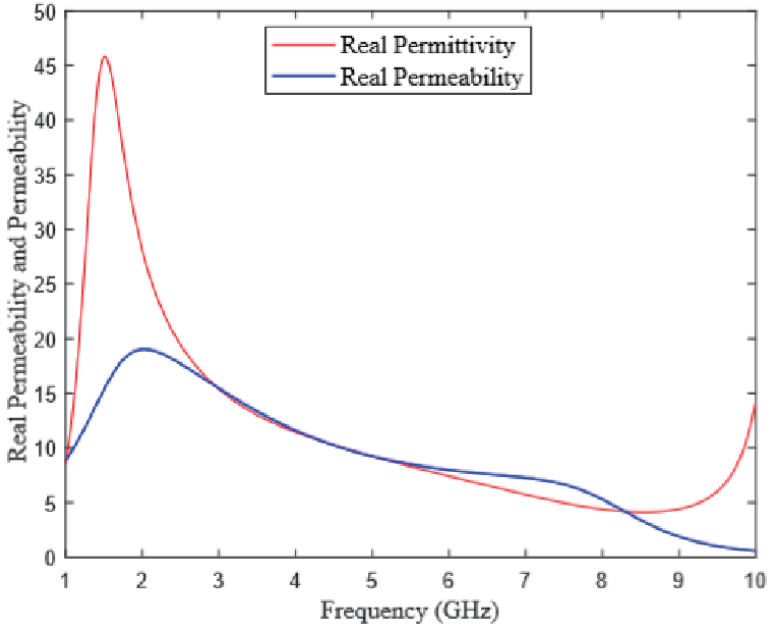

Figure 9. Real part of permittivity and permeability.

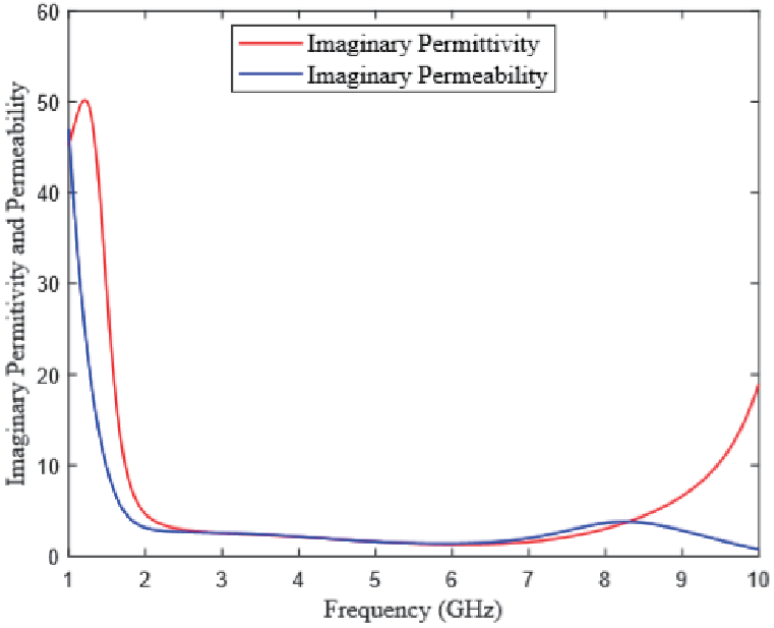

Figure 10. Imaginary part of permittivity and permeability.

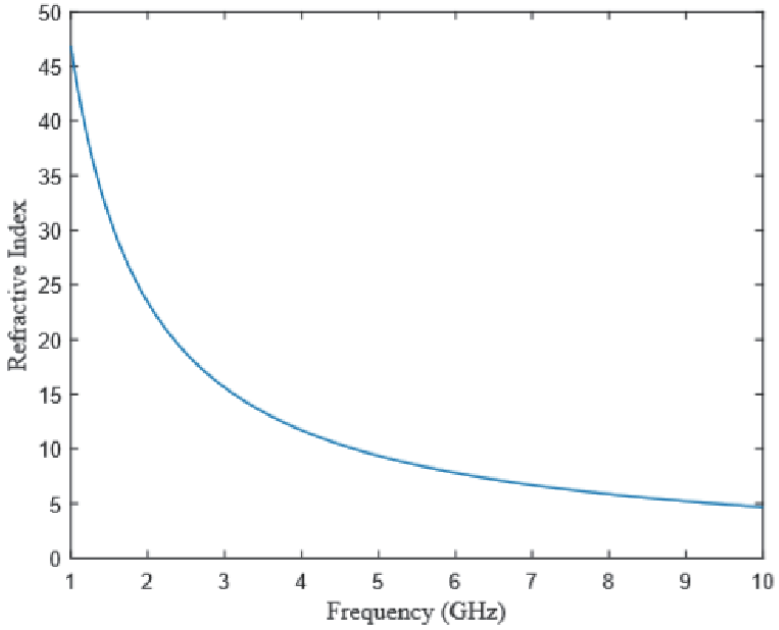

Figure 11. Refractive index vs frequency.

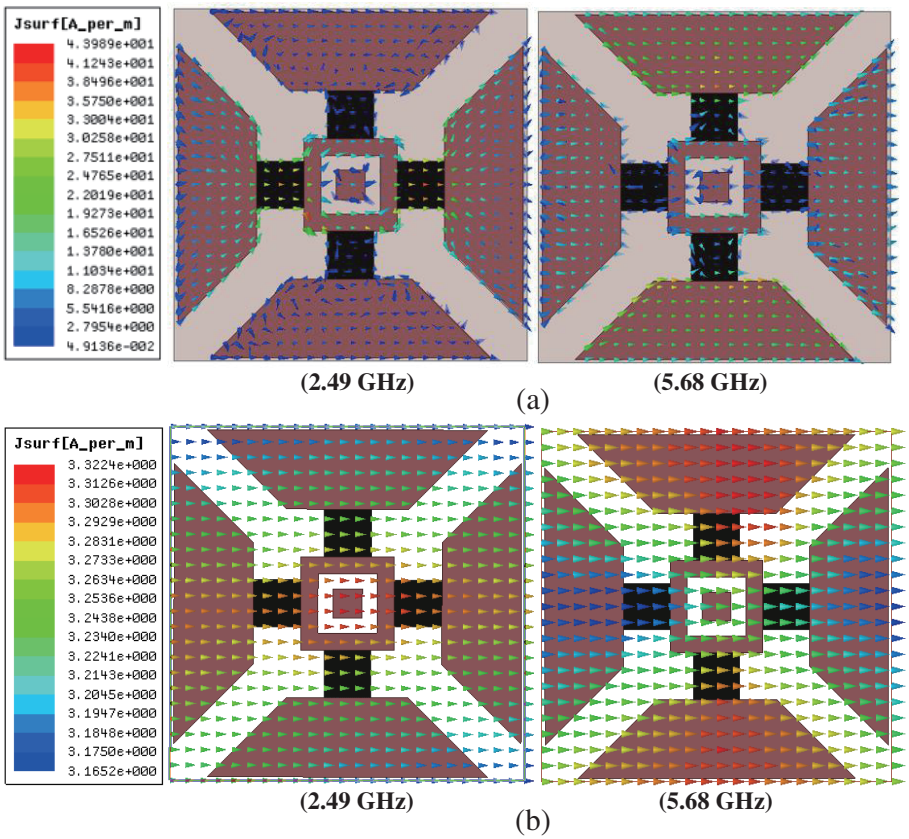

Figure 12. Current distribution (a) top and (b) bottom surfaces at 2.49 and 5.68 GHz of proposed MMA. (a) Upper surface. (b) Lower surface.

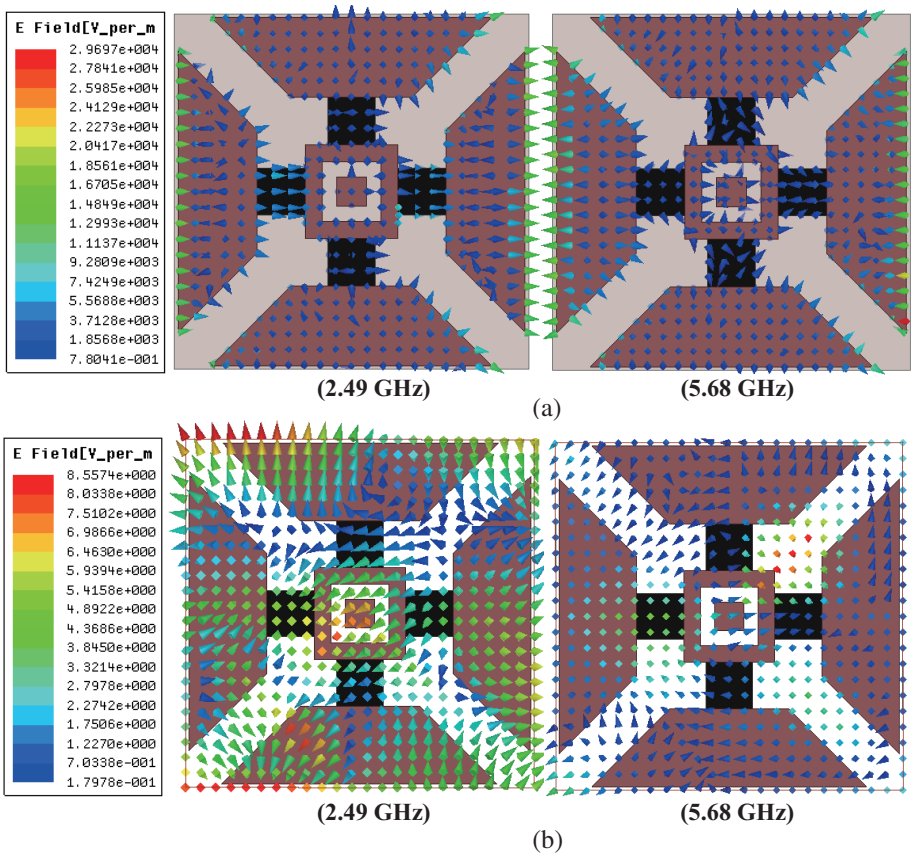

Figure 13. Electric field distribution (a) top and (b) bottom surfaces at 2.49 and 5.68 GHz of proposed MMA. (a) Upper surface. (b) Lower surface.

at certain values or ranges of ε and μ cause η to change abruptly.

$$\eta = \frac{1}{kd}\cos^{-1}\left[\frac{1}{2S_{21}}(1 - S_{21}^2 - S_{11}^2)\right] \tag{9}$$

The electric field distribution is calculated at two different absorption peaks (2.49 and 5.68 GHz). The uppermost and lowermost surface current distributions are antiparallel w.r.t each other as shown in Fig. 12. Magnetic excitation is created due to perpendicular magnetic field because of circulating current, and electric excitation is created due to electric field induced on the surface as depleted in Fig. 13. These strong EM resonances lead to a maximized absorption. This can also be proved by observing Figs. 9 and 10 in which ε_{eff} and μ_{eff} have large deviations at two maximum absorption peaks where magnetic and electrical excitations occur simultaneously.

5. ANALYSIS UNDER OBLIQUE AND NORMAL INCIDENCE

The presented structure is analysed for angle independence using normal and oblique incidences. Firstly, normal incidence is used by keeping the electric field constant and varying wave vector and magnetic field. This is done by keeping vertically polarization ($\phi = 90°$) from horizontally polarization ($\phi = 0°$), and at every 15° increments the reflection coefficient is measured. The absorptivity remains the same throughout even if the polarization angle varies. Hence, the suggested MMA is angle independence, as depicted in Fig. 14.

Secondly, under oblique incident of wave the MMA is analysed at distinct angles from 0° to 90° at each 15° increment for TE and TM polarizations, and absorptivity curves are represented in Fig. 15

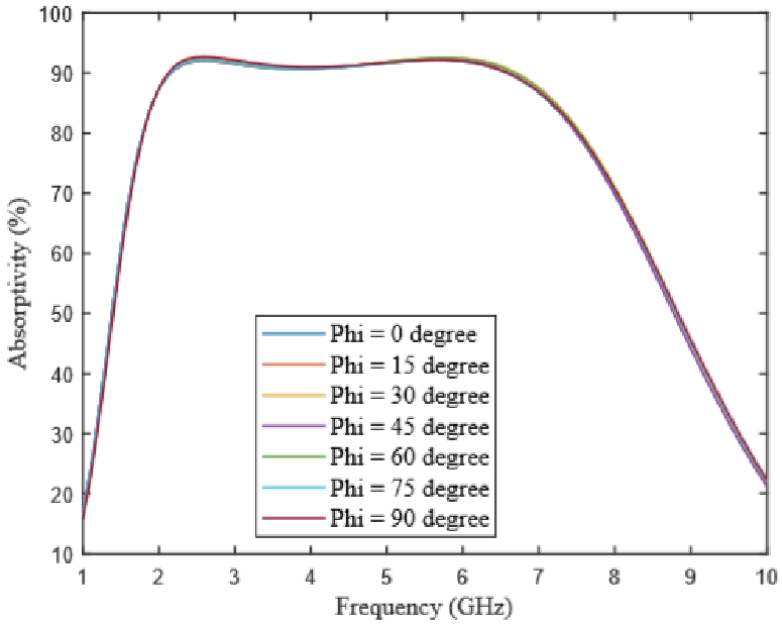

Figure 14. Absorptivity under normal incidence.

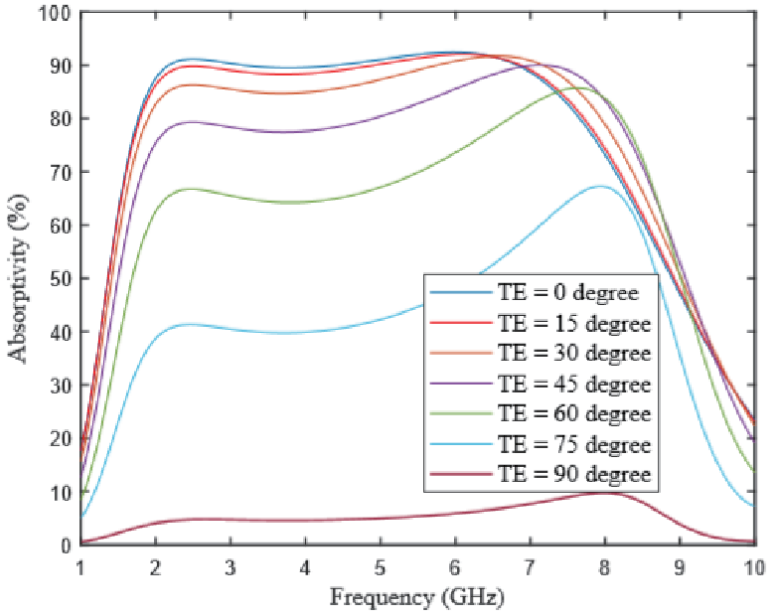

Figure 15. Absorptivity curve under normal incidence for TE polarization.

and Fig. 16, respectively. It is observed that absorptivity decreases when there is increment in the angle of incidence up to 90°.

The presented and already stated state of arts are compared w.r.t size of unit cell, bandwidth, and thickness in Table 1. From the table, it can be determined that the proposed system is compact in dimensions and has wide bandwidth for low frequency region.

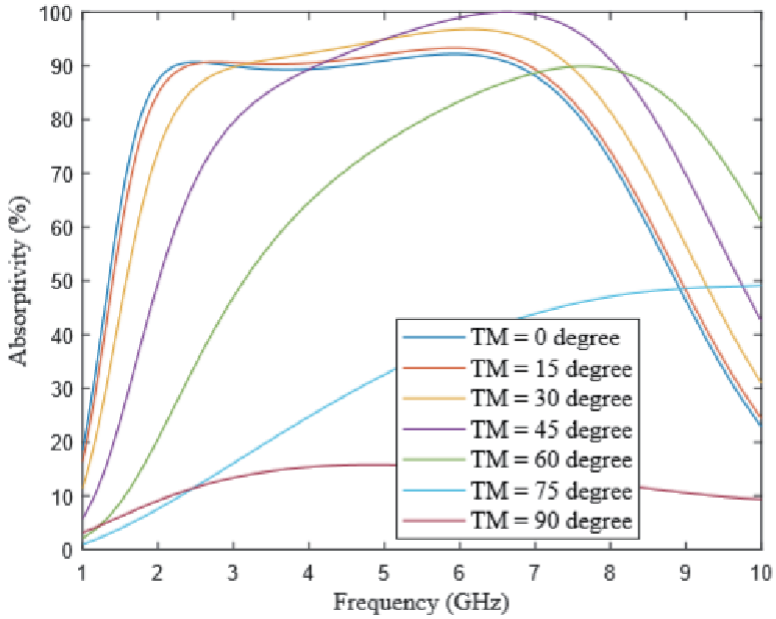

Figure 16. Absorptivity curve under normal incidence for TM polarization.

Table 1. Comparison between presented and stated state of arts MMA.

State of arts	Mid way Frequency (GHz)	Size of single cell (mm)	Thickness (mm)	Bandwidth (GHz)
[15]	19.95	14×14 $(0.93\lambda \times 0.93\lambda)$	2.0 (0.13λ)	0.5
[16]	29.75	12×12 $(1.20\lambda \times 1.20\lambda)$	2.5 (0.25λ)	0.5
[17]	10.25	16×16 $(0.55\lambda \times 0.55\lambda)$	3 (0.10λ)	1.5
[18]	14.65	8.1×8.1 $(0.40\lambda \times 0.40\lambda)$	3.1 (0.15λ)	1.9
[19]	11.15	10×10 $(0.38\lambda \times 0.38\lambda)$	2.5 (0.09λ)	2.7
[20]	28.56	15×15 $(1.53\lambda \times 1.53\lambda)$	4.2 (0.42λ)	3.19
[21]	15.25	10×10 $(1.0\lambda \times 1.0\lambda)$	2.0 (0.20λ)	2.5
Proposed Work	4.41	12×12 $(0.17\lambda \times 0.17\lambda)$	11.67 (0.17λ)	4.4

6. MEASUREMENT SETUP

The MMA with overall area of 6 cm × 6 cm consisting of an array of 5 × 5 unit cells was built on a substrate (FR_4). The resonating structure consisting of copper was built above the substrate sheet. The fabricated sheet and enlarged version of single cell are shown in Fig. 17.

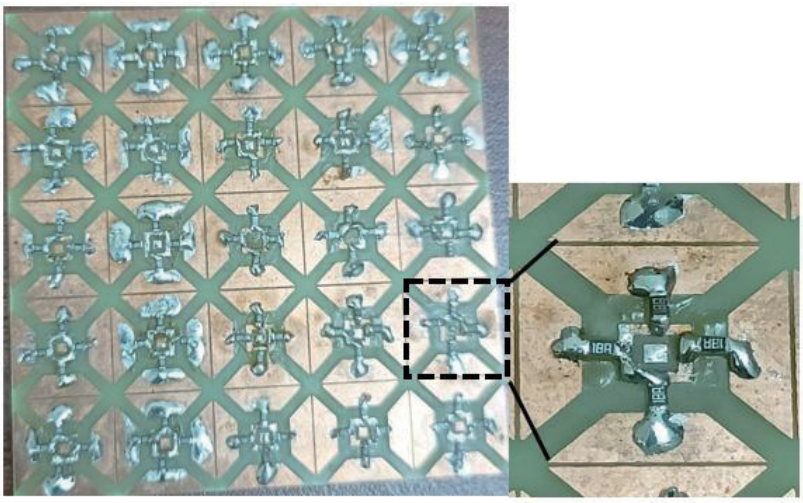

Figure 17. Array of fabricated sheet with enlarged version of single cell.

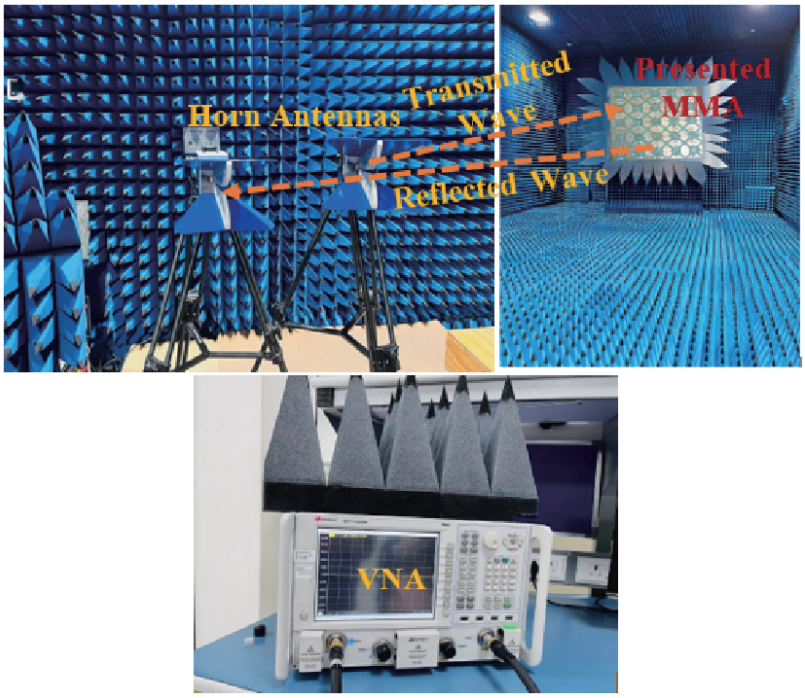

Figure 18. Arrangement inside anechoic chamber.

The fabricated sheet is tested inside an anechoic chamber with the help of two horn antennas and Vector Network Analyzer (VNA). The horn antennas are kept at 1 meter from the sheet where one antenna acts as transmitting antenna, and the other one acts as a receiving one. The arrangement inside the anechoic chamber is shown in Fig. 18.

The testing and simulation plots are measured and shown in Fig. 19. From the plot it is observed that the tested and simulated results are in close agreement.

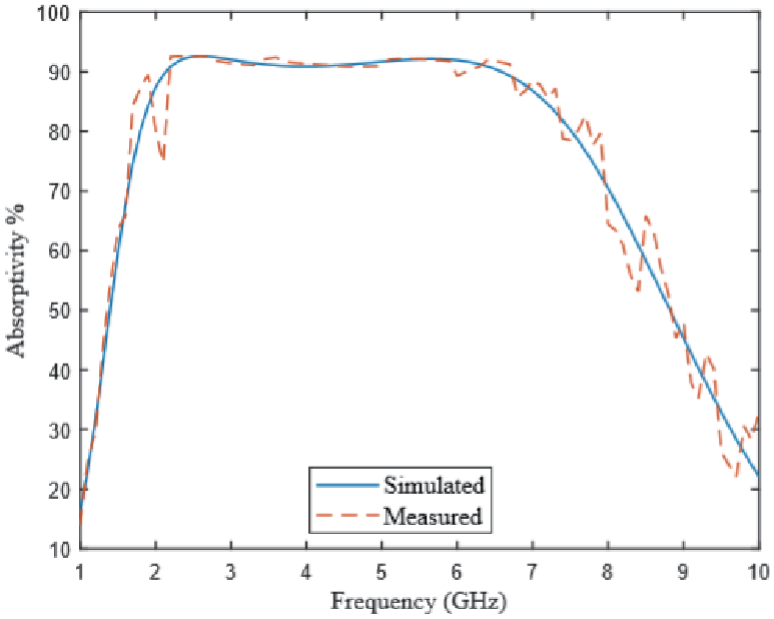

Figure 19. Simulated and measured absorptivity plot.

7. CONCLUSION

The MMA stated in this report is angle independent. The structure is built on an FR_4 substrate having a single cell dimension of 12 mm × 12 mm × 11.67 mm. The layout includes four trapezoids linked with coextensive square through consolidated resistors. The absorptivity is achieved above 90% in the range from 2.21 to 6.61 GHz which conclude wide band of 4.4 GHz. Within this range, two peaks, i.e., 2.21 and 6.61 GHz, are considered for the analysis purpose. Parametric considerations are made in terms of substrate height, height of air aperture, and resistor. The optimized results obtained after performing the parametric study are represented as absorptivity vs frequency plots. To confirm the metamaterial properties acquired by the presented structure, permittivity (ε) and permeability (μ) are considered. Wide band absorption phenomenon is proven with the help of current and electric field distribution. The presented structure is angle independent for phi variation. The fabricated sheet which consists of an array of unit cells is examined inside an anechoic chamber with the help of two horn antennas and VNA. The result obtained from the chamber is compared with the simulated one, and it is observed that they are in close agreements. At last, the presented and already reported state of arts are compared, and it is found that the presented one is used for low frequency with wide bandwidth. The presented MMA finds practical applications in the field of defence for Radar Cross Sections (RCS) reduction.

REFERENCES

1. Metamaterials, E., *Transmission Line Theory and Microwave Applications, The Engineering Approach*, C. Caloz, T. Itoh, 1, A John Wiley Sons Inc. Publication, 2005.
2. Schurig, D. R. S. D., J. J. Mock, and D. R. Smith, "Electric-field-coupled resonators for negative permittivity metamaterials," *Applied Physics Letters*, Vol. 88, No. 4, 041109, 2006.
3. Smith, D. R., W. J. Padilla, D. C. Vier, S. C. Nemat-Nasser, and S. Schultz, "Composite medium with simultaneously negative permeability and permittivity," *Physical Review Letters*, Vol. 84, No. 18, 4184, 2000.
4. Mishra, N., K. Kumari, and R. K. Chaudhary, "An ultra-thin polarization independent quad-band microwave absorber-based on compact metamaterial structures for EMI/EMC applications," *International Journal of Microwave and Wireless Technologies*, Vol. 10, No. 4, 422–429, 2018.

5. Grbic, A., and G. V. Eleftheriades, "Experimental verification of backward-wave radiation from a negative refractive index metamaterial," *Journal of Applied Physics*, Vol. 92, No. 10, 5930–5935, 2002.
6. Lee, S. H., C. M. Park, Y. M. Seo, and C. K. Kim, "Reversed Doppler effect in double negative metamaterials," *Physical Review B*, Vol. 81, No. 24, 241102, 2010.
7. Roy, K. and R. Sinha, "Miniaturized omni-directional ZOR antenna with its co-equal circuit for 5G applications," *Microsystem Technologies*, Vol. 28, No. 11, 2499–2509, 2022.
8. Cai, W., U. K. Chettiar, A. V. Kildishev, and V. M. Shalaev, "Optical cloaking with metamaterials," *Nature Photonics*, Vol. 1, No. 4, 224–227, 2007.
9. Yang, J. J., M. Huang, H. Tang, J. Zeng, and L. Dong, "Metamaterial sensors," *International Journal of Antennas and Propagation*, 2013.
10. Dong, Y. and T. Itoh, "Metamaterial-based antennas," *Proceedings of the IEEE*, Vol. 100, No. 7, 2271–2285, 2012.
11. Mishra, N. and R. K. Chaudhary, "Design and development of an ultrathin triple band microwave absorber using miniaturized metamaterial structure for near-unity absorption characteristics," *Progress In Electromagnetics Research C*, Vol. 94, 89–101, 2019.
12. Roy, K., C. Barde, P. Ranjan, R. Sinha, and D. Das, "A wide angle polarization insensitive multi-band metamaterial absorber for L, C, S and X band applications," *Multimedia Tools and Applications*, 1–13, 2022.
13. Mishra, N., D. K. Choudhary, R. Chowdhury, K. Kumari, and R. K. Chaudhary, "An investigation on compact ultra-thin triple band polarization independent metamaterial absorber for microwave frequency applications," *IEEE Access*, Vol. 5, 4370–4376, 2017.
14. Roy, K., R. Sinha, and C. Barde, "Linear-to-linear polarization conversion using metasurface for X, Ku and K band applications," *Frequenz*, Vol. 76, No. 7–8, 461–470, 2022.
15. Chin, J. Y., M. Lu, and T. J. Cui, "Metamaterial polarizers by electric-field-coupled resonators," *Applied Physics Letters*, Vol. 93, No. 25, 251903, 2008.
16. Ranjan, P., A. Choubey, and S. K. Mahto, "Wide-angle polarization independent multilayer microwave absorber using wind driven optimization technique," *International Journal of Applied Engineering Research*, Vol. 12, No. 19, 8016–8025, 2017.
17. Landy, N. I., S. Sajuyigbe, J. J. Mock, D. R. Smith, and W. J. Padilla, "Perfect metamaterial absorber," *Physical Review Letters*, Vol. 100, No. 20, 207402, 2008.
18. Baqir, M. A., M. Ghasemi, P. K. Choudhury, and B. Y. Majlis, "Design and analysis of nanostructured subwavelength metamaterial absorber operating in the UV and visible spectral range," *Journal of Electromagnetic Waves and Applications*, Vol. 29, No. 18, 2408–2419, 2015.
19. Li, H., L. H. Yuan, B. Zhou, X. P. Shen, Q. Cheng, and T. J. Cui, "Ultrathin multiband gigahertz metamaterial absorbers," *Journal of Applied Physics*, Vol. 110, No. 1, 014909, 2011.
20. Cheng, Y.-Z., R.-Z. Gong, Y. Nie, and X. Wang, "A wideband metamaterial absorber based on a magnetic resonator loaded with lumped resistors," *Chinese Physics B*, Vol. 21, No. 12, 127801, 2012.
21. Ayop, O., M. K. A. Rahim, N. A. Murad, and N. A. Samsuri, "Wideband polarization-insensitive metamaterial absorber with perfect dual resonances," *Applied Physics A*, Vol. 122, No. 4, 316, 2016.